W. W. Gerberich

N. I. Tymiak

J. C. Grunlan

Department of Chemical Engineering
and Materials Science,
University of Minnesota,
421 Washington Avenue, S.E.,
Minneapolis, MN 55455

M. F. Horstemeyer

Center for Materials and Engineering Sciences,
Sandia National Laboratories,
MS 9404,
Livermore, CA 94551-0969

M. I. Baskes

Los Alamos National Laboratory,
MSG 755,
Los Alamos, NM 87545

Interpretations of Indentation Size Effects

For very shallow indentations in W, Al, Au, and Fe-3wt%Si single crystals, hardness decreased with increasing depth irrespective of increasing or decreasing strain gradients. As such, strain gradient theory appears insufficient to explain the indentation size effect (ISE) at depths less than several hundred nanometers. Present research links the ISE to a ratio between the energy of newly created surface and plastic strain energy dissipation. Also, the contact surface to plastic volume ratio was nearly constant for a range of shallow depths. Based on the above, an analytical model of hardness versus depth provides a satisfactory fit to the experimental data and correlates well with embedded atom simulations. [DOI: 10.1115/1.1469004]

Introduction

Material length scales have been a subject of great interest to nearly all engineering and science disciplines. Of large interest to the mechanics/materials community are those material length scales in the 0.1 to 10 μm regime, that have been investigated with small volume torsion wire ([1]) and nanoindentation ([2,3]) experiments. The principle theoretical treatment, with origins in gradient microstructure analysis ([4–7]), has been the use of strain gradient plasticity approaches ([1,3,8–10]). Most effective in tying the materials and mechanics approaches together is a microstructurally based strain gradient analysis propose by Gao et al. [9] and most clearly applied to the indentation size effect by Nix and Gao [3]. This utilized the time-honored strain gradients from geometrically necessary dislocation relationships ([11]) which have been repeatedly verified by experiment ([2,12]).

In the same time frame, propelled by the discoveries of scanning tunneling and atomic force microscopies, principally the physics and chemistry communities addressed much lower contact forces in the nanonewton regime and examined various nanotribology issues. As polymer surfaces came under scrutiny, such probes were elevated to larger μN forces by using stiffer stainless steel cantilevers and previous continuum models are being used to examine adhesive forces ([13]). These involve using the Johnson Kendall Roberts (JKR) ([14]) and Derjaguin Muller Toporov (DMT) ([15]) approaches, and later an incorporation of a Dugdale zone to smoothly obtain the JKR/DMT transition ([16]).

In the region of scale between these atomistic and gradient microstructure regimes, there are possibly one or more phenomena that may contribute to an indentation size effect. It is our intent here to review briefly a number of these effects which can be related to small volumes under contact. This is possible through some recent nanoindentation results ([17]). Specifically, because the previous experimental body of literature ([2,3]) dealing with the indentation size effect emphasized depths of penetration greater than 100 nm and atomic force microscopy had emphasized nm level contacts, we recently evaluated two materials, ⟨100⟩ crystals of aluminum and tungsten, in the regime of 10 to 500 nm ([17]). At the suggestion of Baskes and Horstemeyer [18] who considered the surface to volume ratio to be key, we both experimentally and theoretically determined plastic zone sizes and surfaces of contact to assess the importance of this parameter. At the time neither research group had a physical rationale of why this was important except that atomistic simulations on the one side ([19]) and an experimental evaluation on the other ([17]) strongly suggested that surface to volume, S/V, was the critical parameter. In the present study we group two more materials ⟨001⟩ Fe-3wt%Si and ⟨001⟩ Au with the previous two for critical evaluations of possible contributions to contact forces. First, however, it is appropriate to briefly review the background of two recent studies and a hierarchy of scales that may influence contact forces and therefore any indentation size effect (ISE).

Background

Interest in the indentation size effect (ISE) has resurfaced a number of times; e.g., in 1970 Gane and Cox [20] demonstrated that in Au single crystals that hardness could be increased by a factor of three by decreasing the contact diameter from 10^4 to 10^2 nm. A rekindled interest in the ISE was fostered by the availability of depth sensing instrumentation ([21]) and nearly two decades later, Stelmashenko et al. [22] showed a similar hardness increase at shallow depths in various orientations of single crystal tungsten. They also had a reasoned explanation in terms of the local dislocation hardening due to geometrically necessary dislocations. The hardness, H, was given by

$$H = A\alpha\mu\left[b^2\rho_0 + \frac{b\cot\beta}{d}\right]^{1/2} \tag{1}$$

with A and α nondimensional coefficients of constraint and Taylor hardening, μ the shear modulus, b the burgers vector, ρ_0 a background dislocation density, $\cot\beta$ the wedge shape, and d the diagonal of a Vicker's hardness diamond indenter. Using a reason-

Contributed by the Applied Mechanics Division of THE AMERICAN SOCIETY OF MECHANICAL ENGINEERS for publication in the ASME JOURNAL OF APPLIED MECHANICS. Manuscript received by the ASME Applied Mechanics Division, March 15, 2001; final revision, January 8, 2001. Associate Editor: D. A. Kouris. Discussion on the paper should be addressed to the Editor, Prof. Robert M. McMeeking, Department of Mechanical and Environmental Engineering University of California–Santa Barbara, Santa Barbara, CA 93106-5070, and will be accepted until four months after final publication of the paper itself in the ASME JOURNAL OF APPLIED MECHANICS.

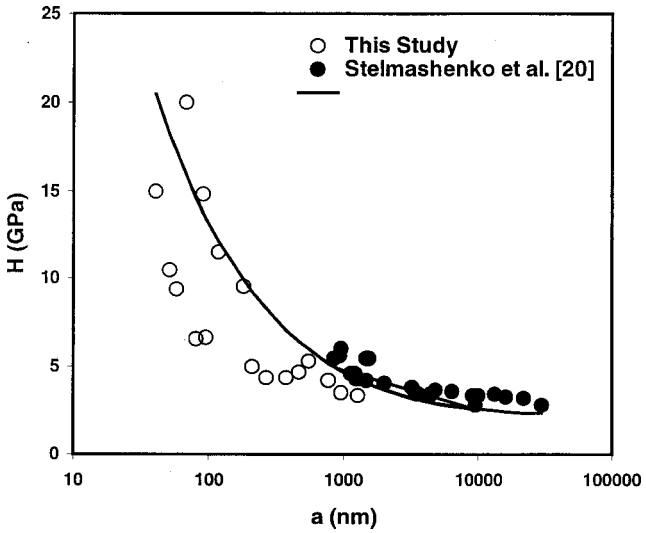

Fig. 1 Hardness as a function of contact dimension in ⟨100⟩ tungsten crystals showing the ISE

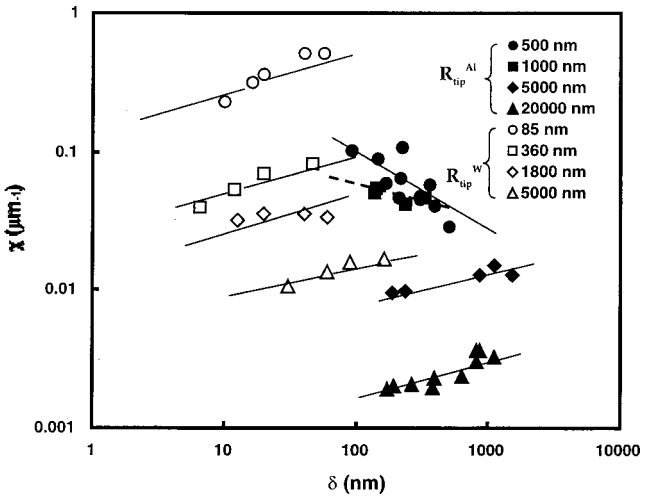

Fig. 2 Average strain gradients, χ, versus depth of penetration, δ, into ⟨100⟩ W (open symbols) and ⟨100⟩ Al (closed symbols) crystals. Four different diamond tip radii used in each case.

able value of $A\alpha \sim 1.5$, the fit to both their data and more recent data for spherical tips ([17,23,24]) is seen in Fig. 1 for single crystal tungsten. This agreement is remarkable considering that the spherical indenters ranged from 85 to 5000 nm in radius, the Vicker's indenter is a sharp, four-sided pyramid and Stelmashenko's data represents five crystal variants while the present data is only for ⟨001⟩. Note that $d/2.5$ is used for the comparison to make equivalent areas of contact for the two types of indenter tips. As some of the low data points for the spherical contact radii, a, represent contact depths of only 10 nm, the scatter observed could be partially a result of surface roughness ([25,26]).

Such findings along with other observed material scale effects led to a phenomenological theory of strain gradient plasticity by Fleck and Hutchinson [1,27] and somewhat later to a mechanism-based strain gradient plasticity theory by Gao et al. [9]. While the mechanism-based theory can ([9]), it is generally recognized that such strain-gradient plasticity theories should not be used at very shallow depths in the vicinity of 100 nm or less. Also, such small size scales become close to the realm of atomistic simulations where depths of penetration of 1 nm have easily been achieved ([28]). These two facts caused us recently to examine the ISE effect in some detail both experimentally ([17]) and computationally ([19]). Regarding the experiments, both average plastic strains, $\overline{\varepsilon_p}$, and strain gradients, $\overline{\chi} = d\varepsilon_p/dc$, were estimated from experimental measures of $\overline{\varepsilon_p}$[1] and plastic zone size, c. As summarized in Fig. 2, the average gradient for a given indentation, $\overline{\chi}$, increased slightly for both small and large spherical tip radii at shallow depths of penetration less than 100 nm. However, deeper penetration depths in the single crystal aluminum produced decreasing values of $\overline{\chi}$ with increasing depths for the sharpest cones but remained spherical-like for the bluntest ones. This can be rationalized partially from simple geometric arguments as Nix and Gao [3] have done for geometrically necessary dislocations emanating from a sharp wedge. The comparison in Fig. 3 suggests that for the spherical tip the average gradient for a spherical contact would be independent of the contact radius (or depth) while the value of χ would fall off as $1/a$ for a sharp wedge. This reinforced current views that continuum-based gradient plasticity models are not appropriate to very small plasticity scales. That is, hardnesses at the shallowest depths were accompanied by strain gradients which were increasing or nearly constant for indentations at greater depth. For that reason an *ad hoc* model was initially determined based upon the observed c/a ratio which was found to first order to be ([17])

$$\left(\frac{c}{a}\right)^2 \simeq \frac{\eta}{a}; \quad \eta = \text{material constant.} \tag{2}$$

Given that even in this small scale range that the plastic zone size is described well by Johnson's cavity model ([29,30]) one can use

$$c = \left[\frac{3P}{2\pi\sigma_f}\right]^{1/2} \tag{3}$$

where P is the applied indentation load and σ_f is an appropriate flow stress. Coupled with Eq. (2) it was shown that a first-order prediction of the ISE could be made ([17]). This still wasn't satisfying, however, as there are no principles of physics or mechanics involved that would explain the indentation size effect.

One can take another look at Eq. (2) and see that if the contact area, πa^2, is coupled to a hemispherical volume of deforming material, $(2/3)\pi c^3$, then a surface-to-volume ratio can be defined as

$$\frac{S}{V} = \frac{3a^2}{2c^3} \tag{4}$$

or

$$\frac{S}{V} = \frac{3}{2\eta} \cdot \frac{a}{c}, \tag{5}$$

Eq. (5) deriving from the size scale parameter of Eq. (2). Given that the a/c ratio was mildly varying by only a factor of two with contact radii up to about 1 μm, this suggests for shallow depths of penetration that the surface to volume ratio defined by Eq. (5) is nearly constant!

At the same time, molecular dynamics simulations using embedded atom method potentials ([19]) were performed on single crystal nickel. With simple shear boundary conditions, Horstemeyer and Baskes ([19]) showed a dependence of the yield stress on the specimen size. It was proposed that dislocation nucleation was a critical phenomena that determined the yield point as a function of volume-to-surface area. This initially caused some confusion between the two research groups until it was clarified as to how volume-to-surface area was being assessed. This is discussed in a note added in proof.

Since the surface-to-volume ratio appeared to play a pivotal role for shallow contacts, we reviewed contact forces over the

[1]These will be addressed in more detail in the experimental section which follows.

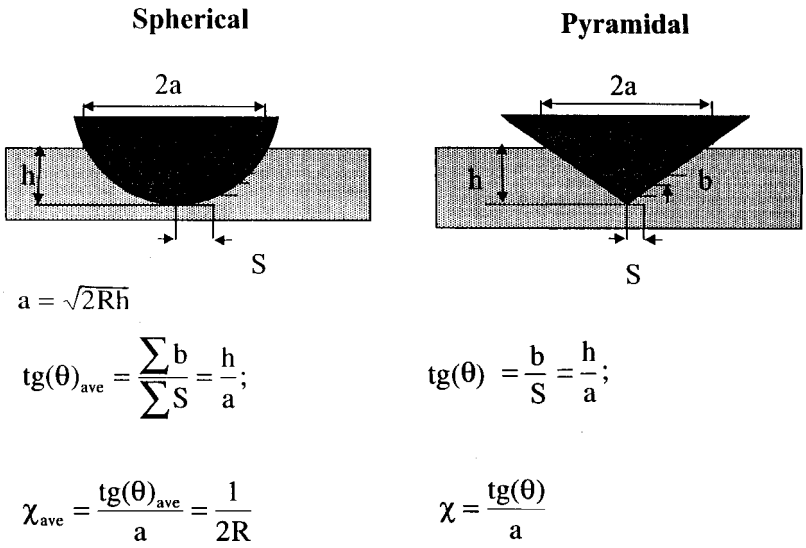

Fig. 3 Schematic of spherical and sharp wedge contacts showing difference in strain gradient dependence on contact shape

scale of interest, $\leqslant 10$ μm, as summarized in Table 1] ([2,3,12,31–41]). For the present study we believe the first three categories represent forces too small to be significant to an ISE. Clearly, adhesive forces can be important particularly to polymer contacts where pull-off forces can be in the 10 μN regime. However, for a number of metal/metal and diamond/metal contacts in laboratory air, the pull-off forces were less than 1 μN representing a force generally less than about three percent of the total.

Consider, next, the level of contact forces associated with surface energy and surface stress. While the forces in a narrow annulus around a surface contact have a limited area of influence, surface energies and excess surface stress may act over areas at least as large as the extent of the plastic zone around the contact. Consider first surface energy, γ_s, which is the work to create new surface as might be related to creating cracks in an oxide film below the contact or new surface as slip steps emerge around the indenter. In another type of experiment on small wires, finite loads are found where creep rates become zero because of the surface energy effect ([33]). Regarding surface stress, the work in elastically deforming surface atoms, this is sufficiently large to trigger surface reconstruction and lattice parameter changes in small spheres ([34–36]). For example, if one considers the surface work only associated with the surface stress, σ_s, this can be converted through the Laplace pressure on a sphere to a change in lattice parameter ([16]). (See Appendix A.) Such observations of lattice parameter changes by TEM electron diffraction have been found ([34–36]). Regarding the next scale level of forces and lengths, there has been a large effort ([38–40,42,43]) in attempting to describe both nucleation and yield forces associated with the onset of plasticity and the arrest of a displacement excursion.

Finally, the well-documented ISE for sharp-wedge tips driven into single and polycrystals and interpreted in terms of length scales associated with strain gradient plasticity needs little introduction here ([2,3]). Such indentation experiments can be described by

Table 1 Contact Forces: a Hierarchy of Scales

Phenomena	Observations	Forces/Energy	Scales
Jump to contact ([3])	STM/AFM	van der Waals	nM/Å
Film dewetting ([32])	AFM	van der Waals versus surface tension (Laplace pressure)	nN/nm
Adhesion ([16])	Surface forces apparatus AFM/nanoindentation	van der Waals, chemical bonding: JKR/DMT	μN/nm
Creep of small volume wires ([33])	Load at zero creep as a function of wire diameter—ISE?	Surface energy, γ_s (work to create a new boundary)	μN/nm
Lattice parameter (a_0) changes ([34–36])	TEM observations show a_0 scales as $1/R$ in spheres		
Thin film yielding under an electrolyte ([37])	Voltage driven surface stress affects nanoindentation induced yielding	Surface stress, σ_s (work to elastically deform surface atoms)	μN/nm
Yield initiation ([38–40])	Drumhead effect; oxide film effect in nanoindentation—ISE?	Film elasticity, image forces, film fracture	μN/nm $\downarrow$ mN
Yield arrest ([24,40])	Displacement excursion in indentation—ISE? TEM, SEM Rosettes	Dislocation array stress field	μN/nm $\downarrow$ mN
Small wire torsion ([41])	Torque versus wire size or	Strain-gradient modified	μN/nm
Indentation size effects (ISE) ([2,3,12])	hardness in sharp-wedge penetration (ISE)	Taylor hardening	$\downarrow$ $\downarrow$ mN μm

Table 2 Details of load (P), displacement (δ), contact radius (a), plastic zone radius (c), hardness (H), and surface to volume (S/V) at the end of yield excursions in ⟨100⟩ Fe-3wt%Si, R_{tip}=70 nm. (Note that only every other data point in Fig. 7(c) is detailed here.)

P μN	δ nm	a nm	c nm	H GPa	H/σ_{ys}	S/V $m^{-1}\times10^{-5}$	$\left(\frac{S}{V}\right)^2\left(\frac{H}{\sigma_{ys}}\right)^3$ $m^{-2}\times10^{-14}$
38	8	33.5	224	10.8	30	1.50	6.08
50	10.5	38.2	258	10.9	30.3	1.27	4.49
60	21	54.2	282	6.5	18.1	1.96	2.28
74	24	58.0	313	7.0	19.5	1.65	2.02
94	40	74.8	353	5.35	14.9	1.91	1.21
100	40.5	75.9	364	5.52	15.3	1.79	1.14
114	48	85.7	389	4.93	13.7	1.88	0.91
118	52	91.1	396	4.53	12.6	2.00	0.80
150	62	104	446	4.43	12.3	1.82	0.62
155	70	114	453	3.79	10.5	2.10	0.51
163	70	114	465	3.98	11.1	1.94	0.52
175	84	132	482	3.19	8.9	2.02	0.39
198	95	146	512	2.95	8.2	2.40	0.31
In ⟨100⟩ Au, R_{tip}=205 nm with only every third data point in Fig. 7(a) detailed:							
16	6.5	51.6	309	1.99	24.9	1.35	2.81
20	7.6	55.8	345	2.04	25.5	1.14	2.15
21	9.0	60.7	354	1.81	22.6	1.25	1.80
30	12	70.1	423	1.94	24.2	0.97	1.33
48	14	75.8	535	2.66	33.2	0.56	1.15
40	15.5	79.7	489	2.00	25	0.81	1.04
50	16.5	82.2	546	2.35	29.4	0.623	0.986
44	18	85.9	512	1.90	23.8	0.825	0.918
48	20	90.6	535	1.86	23.2	0.804	.807
47	22	95.0	530	1.66	20.7	0.989	.733
58	25	101	588	1.81	22.6	0.832	.799
62	27	105	608	1.79	22.4	0.759	.647
72	30	111	656	1.86	23.3	0.654	.541
70	33	116	646	1.65	20.6	0.749	.490
71	34	118	651	1.62	20.2	0.757	.472
88	40	128	725	1.71	21.4	0.645	.408
92	47	139	741	1.52	19	0.712	.348
98	52	146	765	1.46	18.2	0.714	.307

$$\frac{H}{H_0}=\sqrt{1+\frac{\delta^*}{\delta}} \tag{6}$$

where H_0 is the hardness in the absence of strain gradients, δ^* is a length scale parameter, and δ is the depth of penetration. We would like to point out two aspects. First, the form of Eqs. (1) and (6) are identical with $H_0=A\alpha\mu/c_1$ and $\delta^*=c_2b$ but the interpretation is different. Stemashenko [22] originally only considered hardening due to geometrically necessary dislocations while Nix and Gao [3] considered a flow stress given by

$$\sigma_f=\sigma_{ys}\sqrt{f^2(\varepsilon)+\delta^*\chi_{\rho G}} \tag{7}$$

with hardening a function of both strain and strain gradient. The second point is that both average strain and average strain gradients tend to increase with increasing depth for ''sharp tips'' at very shallow depths or for larger spherical tips at all depths. See Fig. 2. Since Eq. (7) implies larger flow stresses for deeper depths of penetrations with spherical tips, this did not seem to explain the shallow penetration data of Fig. 1. Some corroboration of this at light loads was found by Yasuda et al. [43] who documented that the dislocation density of the isotropic plastic zone increased with increasing depths of penetration. For that reason they rejected the model of Stelmashenko et al. [22] which only emphasized the dislocation density aspect. The above aspects led us to the conclusion that for very shallow indents that a model based upon surface, S, to volume relation, V, considerations might be promising.

Experimental

Details of the loads, displacements, plastic zones, contact radii, strains, and strain gradients are given elsewhere ([17]) for ⟨100⟩ Al and ⟨100⟩ W. For this study also analyzed in the same way were ⟨100⟩ Au [44] and ⟨100⟩ Fe-3wt%Si ([17–23]) single crystals. Justification in terms of geometrically necessary dislocations gave strains as δ/c and average gradients, $\overline{\chi}$, as δ/c^2. Tip radii of 500, 1000, 5000, and 20,000 nm were used for the ⟨100⟩ Al, 85, 360, 1800, and 5000 nm for the ⟨100⟩ W and single tips of 70 nm and 205 nm for ⟨100⟩ Fe-3wt%Si and Au, respectively. In one instance a 700 nm spherical diamond tip was used for tungsten as noted. Since the Fe-3wt%Si and Au were not published elsewhere, these are shown in detail in Table 2. The Fe-3wt%Si tip used to determine strain gradient was relatively sharp and since it was a three-sided Berkovich, an appropriate area function for the transition from spherical to triangular was utilized to define contact area and an effective radius of contact.[2] For further justification of the strain and strain gradients used, we had accomplished a numerical analysis of a very shallow contact into simulated nanocrystalline tungsten with a yield strength of 4 GPa and a modulus of 400 GPa. The 500 nm spherical tip at the end of a 90-deg cone was driven into the tungsten to a depth of 167 nm. The approach ([45]) used was an explicit, numerical formulation utilizing the finite difference method for a three-dimensional model based on large deformation, elastoplastic contact mechanisms. Moving boundaries and quasi-static states were handled with an updated Lagrangian approach. The resulting Mises strain as a function of distance from the tip is shown in Fig. 4 with strains up to about 0.5. The average strain in the zone was 0.154 whereas if we consider δ/c it is 0.209 for this 800 nm plastic zone. Further, one can curve fit and show the average gradient in the zone to be about 5×10^5 m^{-1} while δ/c^2 is 2.6×10^5 m^{-1}. The difference between

[2]Previously, we had shown for different shapes of indenters that Eq. (3) gave an appropriate account of measured plastic zones ([30]). While such a shape change at deeper depths will not affect the surface to volume ratio or mean pressure determinations, this may bias their relationship with displacement. The reader should be aware that such variance would cause a small shift in some of the data plots where depth to the one-third power is encountered.

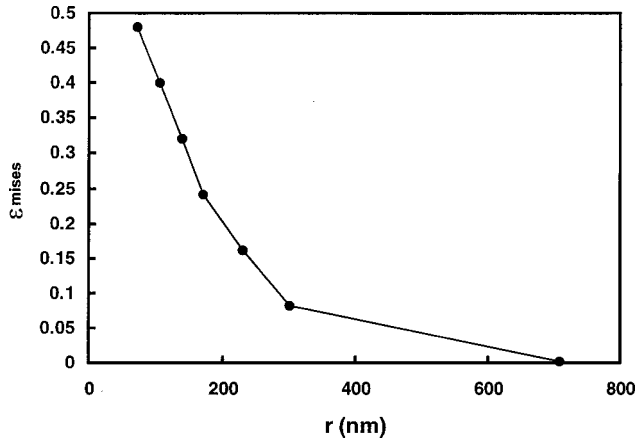

Fig. 4 Mises strain as a function of distance, *r*, from indenter tip for a three-dimensional finite difference numerical analysis

these and the $1/2R$ gradient of 10^6 m^{-1} indicated in Fig. 3 is due to the ''gage length'' basis of ''*c*'' and ''*a*'' used, the former being preferred.

Theoretical

To understand how important the surface to volume, S/V, ratio is, estimates of surface work and the volume work associated with plastic deformation under a contact are in order. Considering first the surface work, a number of contributions including both surface energy and surface stress are examined. For the general case the total work associated with creating either new area, dA, or new surface energy, $d\gamma$, can be written as

$$gdA = \gamma dA + Ad\gamma \tag{8}$$

using Maugis' terminology ([16]). He goes on to demonstrate that for a surface of N atoms with an area $A = Na_0$ that the surface work is due to both elastically stretched bonds, da_0, and new numbers of atoms exposed, dN, giving

$$gdA = \gamma a_0 dN + \sigma_s N da_0 \tag{9}$$

where γ is surface energy and σ_s is the surface stress. With the definition of strain dA/A being both plastic, ε_p, and elastic, ε_ε, it follows that ([46])

$$g = \gamma \frac{\varepsilon_p}{\varepsilon} + \sigma_s \frac{\varepsilon_E}{\varepsilon} \tag{10}$$

where ε is the total strain. Thus, the total surface work, W_s, is made up of new area associated with irreversible plastic work as well as elastically stretched bonds associated with reversible work. There are a number of possible contributions to indentation surface work as follows:

(i) creating new surface associated with straining material outside the contact. This could involve oxide fracture, γ_s^{ox}, oxide/metal interface fracture, γ_i^{m-ox}, and/or slip step emergence in the metal itself, γ_s^m:

$$W_s^i = \pi(c^2 - a^2)[f_1\gamma_s^{ox} + f_2 w^{m-ox} + f_3\gamma_s^m];$$
$$w^{m-ox} = \gamma_s^m + \gamma_s^{ox} - \gamma^m. \tag{11a}$$

(i) creating surface by fracture of oxide, γ_s^{ox}, or the metal/oxide interface, $m-ox$, giving

$$W_s^{ii} = \pi a^2[f_4\gamma_s^{ox} + f_5 w^{m-ox}]; \quad w^{m-ox} = \gamma_s^m + \gamma_s^{ox} - \gamma_s^{mox}. \tag{11b}$$

(i) formation of adhesion between the diamond indenter-tip and the oxide surface film:

$$W_s^{iii} = \pi a^2[f_6 w^{d-ox}]; \quad w^{d-ox} = \gamma_s^d + \gamma_s^{ox} - \gamma_s^{dox}. \tag{11c}$$

(i) surface stress deformation work outside the area of contact

$$W_s^{iv} = \pi(c^2 - a^2)[f_7\sigma_s]. \tag{11d}$$

Note here that the interfacial energies, w, are the Dupré works of adhesion and the f_i are the fraction of areas contributing. Since $f_1 = f_4$, $f_2 = f_5$, one can show to first order for an annulus of plastic deformation of $c \sim 2a$ that these sum to

$$W_s^{\text{total}} \sim \sum_i w_s^i \sim 4\pi a^2 \overline{f}[\gamma_s^{ox} + \gamma_s^m];$$
$$\gamma_s^{ox} \sim \gamma_s^m, \overline{f} \simeq 0.125$$
$$W_s^{\text{total}} \sim \pi a^2 \gamma_s^m. \tag{12}$$

Further simplifying assumptions were that we could ignore surface stress, that f_1 and f_2 for fractured oxide or metal/oxide interfaces were about a quarter of the contact area fraction under the indenter, f_6, and that $\gamma_s^d \sim \gamma_s^{ox} > \gamma^{dox}, \gamma^{mox}$. While one can easily argue the details, the simple relation we desired here is that to first order the total surface work is given by the product of the contact area and metal surface energy.

Next, consider the volume deformation associated with plastic work, W_p. From a continuum standpoint W_p can be defined in terms of the plastic volume, V, and the tensile yield stress σ_{ys}, for an elastic-perfectly plastic material giving

$$W_p = V\int_0^{\varepsilon_p} \sigma_{ys} d\varepsilon_p. \tag{13a}$$

Defining an incremental strain as before $d\varepsilon_p = d\delta/c$ and noting that the hemispherical plastic volume would be $(2/3)\pi c^3$ one sees that

$$W_p = V\int_0^{\delta} \frac{\sigma_{ys}}{c} d\delta = \frac{2}{3}\pi c^2 \sigma_{ys}\delta. \tag{13b}$$

There is a hidden assumption that ''*c*'' is constant but recent experiments ([47]) with direct AFM imaging demonstrate a substantial plastic zone prior to the yield excursion. An alternative way of examining this work is to define an incremental work similar to that proposed by Cheng and Cheng [48]. Using Eq. (3) with $\sigma_f \sim \sigma_{ys}$ gives

$$dW_p = Pd\delta = \frac{2\pi\sigma_{ys}c_i^2}{3} d\delta \tag{13c}$$

with c_i the instantaneous plastic zone size. If we assume that $c_i = c =$ constant, then

$$W_p = \frac{2\pi\sigma_{ys}c^2}{3}\int_0^{\delta} d\delta = \frac{2}{3}\pi c^2\sigma_{ys}\delta. \tag{13d}$$

It is seen that (13*b*) and (13*d*) are identical. Further corroboration is taken from the dislocation theory by assuming that concentric loops of length from near zero to c ($c/2$ on average) move down glide cylinders to produce work under a shear stress, τ_{ys}. This gives

$$W_p = \underset{\substack{\text{number}\\ \text{of loops}}}{\frac{\delta}{b}} \cdot \underset{\substack{\text{force per unit length}\\ x \text{ average loop length}}}{\tau_{ys} b \pi c} \cdot \underset{\text{distance moved}}{c} = \pi c^2 \tau_{ys}\delta. \tag{13e}$$

Taking $\tau_{ys} \sim (2/3)\sigma_{ys}$ makes (13*b*) = (13*d*) = (13*e*). Still since $\overline{c} < c$ but only slightly and the displacement excursions have been shown to be about half the total displacement ([40]), it follows that a good estimate of the plastic work is

$$W_p \simeq c^2 \tau_{ys}\delta_{exc}. \tag{14}$$

Using the total displacement with Eqs. (12) and (14), the surface to volume work ratio is given by

$$\frac{W_s}{W_p} = \frac{2\pi\gamma_s^m}{\tau_{ys}\delta}\left(\frac{a}{c}\right)^2. \tag{15}$$

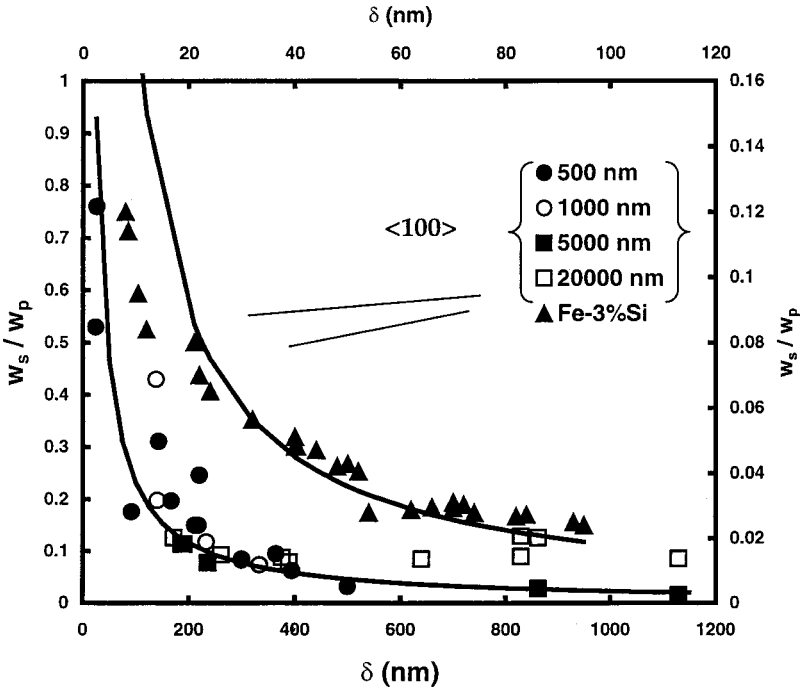

Fig. 5 Ratio of surface to volume works as a function of indentation depth into ⟨100⟩ Al and ⟨100⟩ Fe-3wt%Si single crystals

What this illustrates is that if the a/c ratio is nearly constant at shallow penetration, then the portion of surface work resisting penetration rapidly decreases with increasing depth of penetration as γ_s^m and τ_{ys} are constant. Back at Eq. (5) it was suggested that for relatively shallow depths of penetration that S/V may be nearly constant. We next examine this and the surface work argument as to how this gives rise to an indentation size effect.

Results and Discussion

First, both W_s and W_p were determined from Eqs. (12) and (14) using either calculated values of c and a as for Fe-3wt%Si or AFM imaged values for aluminum crystals. Values for shear yield stress were 180 MPa for Fe-3wt%Si and 30 MPa for aluminum. These data as shown in Fig. 5 illustrate two points. First, for very shallow penetrations the surface work can be a significant portion of the total work. While a surface work contribution of 10% may not seem significant we believe the values in Fig. 5 to be an underestimate of the true ratios. After these calculations were made it was suggested that the surface area could easily be larger than the πa^2 used if the vertical surface steps associated with both oxide fracture and slip band emergence were used, e.g., pile up. Consider just a native oxide fracture of 3 nm, and approximately half of the dislocation loops emerging at the free surface to fracture oxide. One can show that the surface steps as long traces through the plastic zone could produce a new area about three times larger than πa^2. Second, the solid curves are Eq. (15) with c/a a single value of three for both materials. Going back to Eq. (5) then this does strongly imply that if the size scale parameters were relatively unchanged, that the surface to volume ratios would also be constant and near to each other. From data of previous ([17,23,44]) and present investigations, S/V values were calculated and are shown as a function of depth in Fig. 6. Here it is remarkable to see how constant the S/V values are up to depths of about 200 nm (note the scale difference for aluminum). The slightly greater scatter for Al and W can be partially attributed to using four different tip radii in each case. As to the average S/V

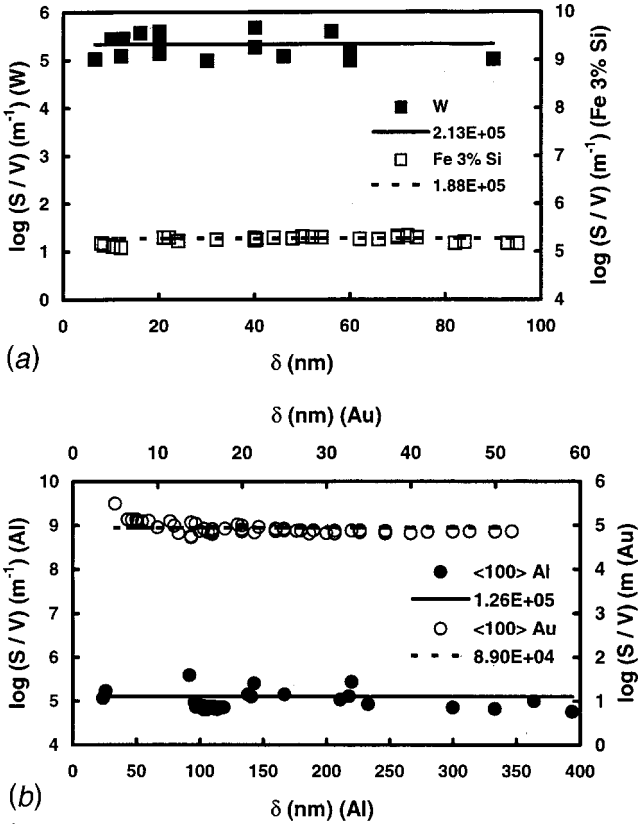

Fig. 6 Surface-to-volume ratio, defined by projected contact area to plastic volume, as a function of indentation depth for (*a*) ⟨100⟩ W and ⟨100⟩ Fe-3wt%Si; (*b*) ⟨100⟩ Au and ⟨100⟩ Al single crystals. Solid and dashed curves represent the mean *S/V* values for each material. Note the different scales for the two materials in (*b*).

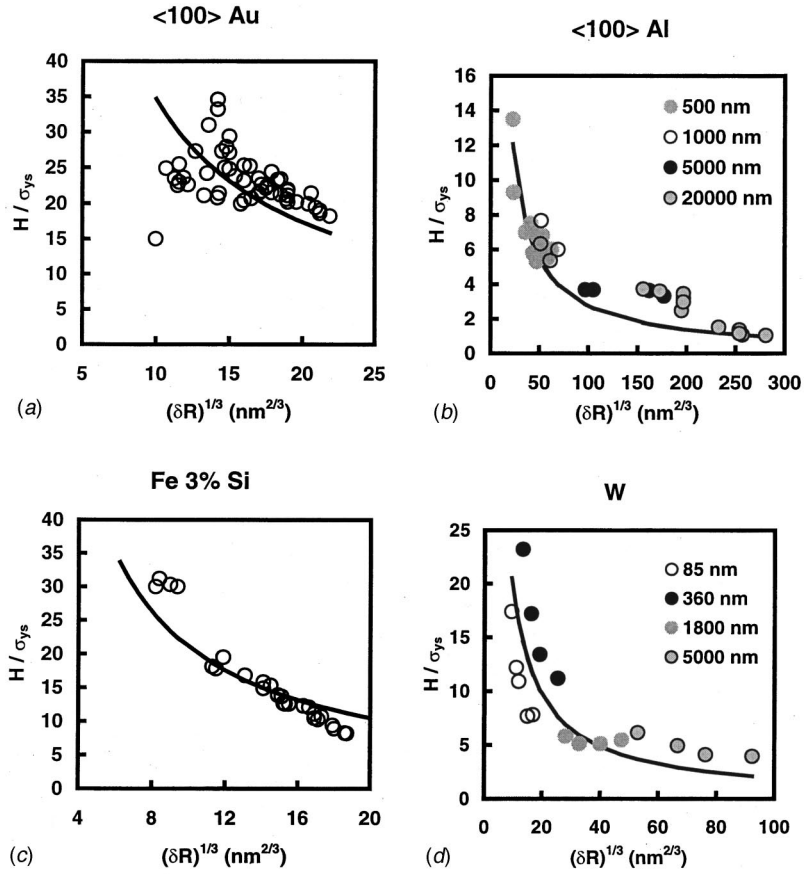

Fig. 7 Fit of the proposed model (Eq. (19)) for four ⟨100⟩ oriented single crystals. Single tips of 205 nm and 70 nm radii used in (*a*) and (*c*), respectively; multiple spherical tips with radii noted used in (*b*) and (*d*)

values, these tended to be in the $(1\text{-}2)\times 10^5$ m^{-1} regime for all four materials, the ranking of which we consider later.

With $S/V\sim$constant for a given material at shallow depths, it was straightforward to arrive at an ISE. Defining $S/V=3a^2/2c^3$, it is seen that

$$\left(\frac{S}{V}\right)^{2/3}=\frac{(3/2)^{2/3}a^{4/3}}{c^2}. \tag{16}$$

For plastic contacts of a spherical tip Johnson [29] takes $a^2\sim 2\delta R$ which is nearly the geometric value and combining this with the mean pressure defines hardness as

$$H\simeq\frac{P}{\pi a^2}\simeq\frac{P}{2\pi\delta R}. \tag{17}$$

But we had already demonstrated that the plastic zone could be given by Johnson's cavity model, Eq. (3), so that by eliminating P, (17) becomes

$$H=\frac{\sigma_f c^2}{3\delta R}. \tag{18}$$

It is seen with S/V constant, Eq. (16) and $a^2\sim 2\delta R$ can be used to eliminate c^2 in Eq. (18) giving

$$H\simeq\frac{\sigma_f}{\left(\frac{S}{V}\right)^{2/3}}\cdot\frac{1}{(3\delta R)^{1/3}}. \tag{19}$$

H/σ_f is shown versus $(\delta R)^{1/3}$ for all four materials in Fig. 7. With the average values of S/V from Fig. 6, it is also seen that the model fits the data both in terms of the ISE but also appropriately ranking the tip radius effect. It should be mentioned here that σ_f was taken as the yield stress for Au, Al, and Fe-3 wt%Si but was taken as the flow stress for W as discussed by Bahr et al. [23]. As seen from Eq. (19), $(S/V)^2\ (H/\sigma_{ys})^3$ should collapse all of the data when shown versus $(\delta R)^{-1}$. Such a master plot in Fig. 8

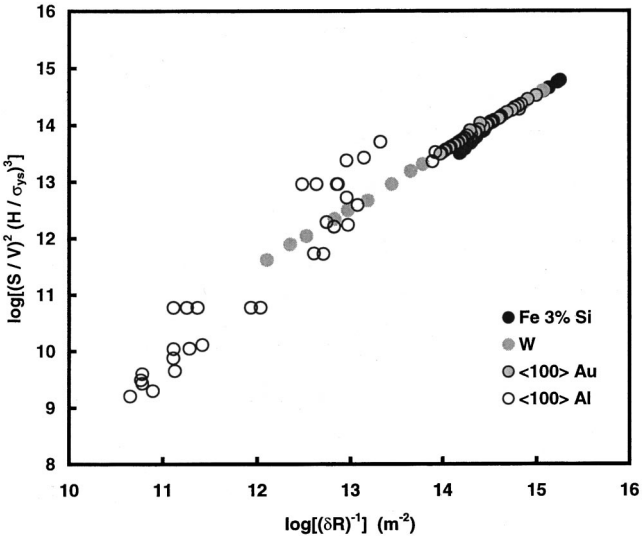

Fig. 8 Master plot of Eq. (19) for all materials

Table 3 Scaling of flow stress, surface energy, and elasticity to surface/volume ratio

	Au	Al	Fe	W
γ_s N/M†	1485	980	1950	2800
c_{11}, Pa$\times 10^{-10\dagger}$	18.6	10.8	24.2	52.1
σ_f, Pa$\times 10^{-6}$	80	60	360	860
$\sigma_f/c_{11}\times 10^4$	4.3	5.6	14.9	16.5
$\sigma_f^2/\gamma_s c_{11}$, m^{-1}	23	34	275	507
S/V, m$^{-1}\times 10^{-5}$	0.89	1.26	1.88	2.13

†Data from Hirth and Loethe, Ref. [49].

does this but it is seen that a break in the curve appears at a δR of about 3×10^{-13} m^2 for the aluminum data which involved the deeper penetrations. For the 1000 nm tip radius this represents a penetration depth of 300 nm, just about where the surface to volume ratio ceases to be constant in Fig. 6. It appears then that a different mechanism for the ISE may take place at deeper penetration depths where the surface work contribution is minimal.

One final discussion point is the apparent ranking of average S/V ratios in Fig. 6. One way is through the physical properties of the materials as given in Table 3 [49]. Here it is seen that the two lowest surface energy metals have the lowest S/V ratios which seems counterintuitive. On the other hand, the ratio of flow stress to the elastic stiffness constant, c_{11}, does seem to rank order the S/V values. In addition the elastic strain energy density clearly scales with σ_f^2/E so that the greater stored elastic energy about indents into the higher yield strength materials may be playing an additional role in requiring an increased surface-to-volume ratio. If that is the case then dimensional analysis would imply that $\sigma_f^2/\gamma_s c_{11}$ should scale with S/V as these both have m^{-1} units. Comparing the last two rows of Table 3 shows this to be the case on a semi-log basis.

Note added in proof: Sometime after this paper was 95 percent complete our respective research groups contacted each other and found that our surface to volume concepts didn't even fit on the same page. It became readily apparent that we had utilized two different definitions of volume wherein V_B represented the volume displaced by the indenter whereas V_G represented the plastic volume involved in volume work. To properly compare our data we needed to define $(V/S)_B$ for our spherical indentations. For a spherical segment indenting a planar surface, V and S are defined by geometry, giving

$$\left[\frac{V}{S}\right]_B = \frac{\frac{\pi\delta^2}{3}[3R-\delta]}{2\pi R\delta} = \frac{\delta}{2} - \frac{\delta^2}{6R} \approx \frac{\delta}{2}; \quad R \gg \delta \tag{20}$$

where for Baskes and Horstemeyer V_B is in terms of the indenter displaced volume. For comparison, we report yield strength as estimated from hardness ($\sigma_{ys}\sim H/3$) normalized on Young's modulus E. From Eq. (19), this combined with (20) gives

$$H = \frac{\sigma_{ys}^0}{\left(\frac{S}{V}\right)_G^{2/3}} \cdot \frac{1}{\left(6\left[\frac{V}{S}\right]_B R\right)^{1/3}}. \tag{21a}$$

Here, we distinguish the bulk yield strength, σ_{ys}^0, from the yield strength, σ_{ys}, that would be obtained from $H/3$, thereby involving the ISE. Taking $H/3$ as σ_{ys} and normalizing on modulus gives

$$\frac{\sigma_{ys}}{E} = \frac{\sigma_{ys}^0}{3E\left(\frac{S}{V}\right)_G^{2/3}} \cdot \frac{1}{\left(6R\left[\frac{V}{S}\right]_B\right)^{1/3}}. \tag{21b}$$

Note for a given material that σ_{ys}^0/E is constant and $[S/V]_G$ is approximately constant at shallow depths (Fig. 6). The result for a constant tip shape is that σ_{ys}/E should be proportional to $[V/S]^{-0.33}$ whereas Horstemeyer and Baskes originally reported an exponent of -0.38. This is further remarkable since in reexamining data left out of the original analysis, those data shown along with a new least-squares fit give a slope equal to -0.33 in near perfect agreement with the $-1/3$ slope predicted by (21*b*). As is seen in Fig. 9, there is now a reasonable qualitative agreement between the two sets of data.

Summary and Conclusions

From examination of average strains and strain gradients as a function of indentation depth, this reinforces previous views that gradient plasticity models do not apply at very shallow depths. An alternative model for depths up to several hundred nanometers is

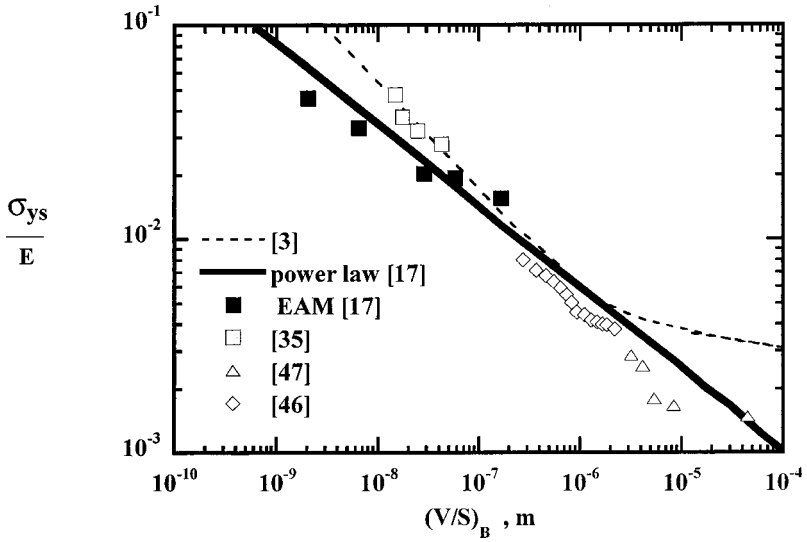

Fig. 9 Incorporation of the Baskes and Horstemeyer definition of volume to surface ratio, $(V/S)_B$, for comparison of atomistic simulations to the present data: solid line is a power-law fit with -0.38 slope similar to Eq. (21*b*)

proposed in terms of a surface work and plastic volume work concept. The critical feature is the $(S/V)_G$ where S is the projected contact area and V_G is the plastic volume under the contact. It is further concluded that

1 The functional dependence of both average strain and average strain gradient on indentation depth is even qualitatively different for spherical versus sharp wedge indenters.

2 At very shallow depths average strain gradients increase with increasing indentation depth for all spherical tip radii and even for larger spherical tip radii at depths deeper than 100 nm.

3 Assessment of surface and volume works demonstrate that both of these can be fundamentally important at shallow depths of indentation where size scales are small.

4 For shallow depths of indentation the $(S/V)_G$ is nearly independent of depth.

5 The proposed model based upon a constant $(S/V)_G$ model predicts normalized hardness to decrease as $(\delta R)^{-1/3}$. This fits $\langle 100 \rangle$ single crystal data for Au, Al, Fe-3wt%Si, and W.

Acknowledgments

We greatly appreciate use of a high-load transducer and the aluminum single crystal provided by Hysitron, Inc. Research support from NSF-DMI-99871863 for two of us (NIT and WWG) from a Graduate School Fellowship for one of us (JCG) and from a grant by Seagate Technology through MINT for one of us (WWG) is gratefully acknowledged.

Appendix

Surface Stress as a Work Term. Using the Laplace pressure to find the effect of surface stress on the lattice parameter change in nanometer scale particles, Maugis [16] finds

$$\sigma_s = \frac{R}{2}\Delta p = -\frac{R}{2\chi_c}\frac{\Delta V}{V} = -\frac{3}{2}\frac{R}{\chi_c}\frac{\Delta a}{a} \qquad (A.1)$$

where the pressure change is interpreted in terms of the relative volume change, $\Delta V/V$, and the compressibility, χ_c. Defining $\Delta a/a$ as a lattice strain, ε, and noting that the bulk modulus, K, is the inverse of compressibility, this gives the surface stress as

$$\sigma_s = \frac{3}{2}KR\varepsilon. \qquad (A.2)$$

By measuring lattice strains via electron diffraction in small spheres, Vermaak et al. [34–36] determined σ_s in Au, Ag, and Pt to range from about 1.2 to 2.6 J/m^2.

References

[1] Fleck, N. A., and Hutchinson, J. W., 1993, "A Phenomenological Theory for Strain Gradient Effects in Plasticity," J. Mech. Phys. Solids, **41**, pp. 1825–1857.
[2] Ma, Q., and Clarke, D. R., 1995, "Size Dependent Hardness of Silver Single Crystals," J. Mater. Res., **10**(4), pp. 853–863.
[3] Nix, W. D., and Gao, H., 1998, "Indentation Size Effects in Crystalline Materials: A Law for Strain Gradient Plasticity," J. Mech. Phys. Solids, **46**(3), pp. 411–425.
[4] Aifantis, E. C., 1984, "On the Microstructural Origin of Certain Inelastic Modes," ASME J. Eng. Mater. Technol., **106**, pp. 326–330.
[5] Zbib, H., and Aifantis, E. C., 1989, "On the Localization and Post Localization of Plastic Deformation—Part I: On the Initiation of Shear Bands," Res. Mech., pp. 261–277.
[6] Zbib, H., and Aifantis, E. C., 1989, "On the Localization and Post Localization of Plastic Deformation—Part II: On the Evolution and Thickness of Shear Bands," Res. Mech., pp. 279–292.
[7] Zbib, H., and Aifantis, E. C., 1989, "On the Localization and Post Localization of Plastic Deformation—Part III: On the Structure and Velocity of Postevin–Le Chatelier Bands," Res. Mech., pp. 293–305.
[8] Shu, J. Y., and Fleck, N. A., 1998, "The Prediction of a Size Effect in Microindentation," Int. J. Solids Struct., **35**(13), pp. 1363–1383.
[9] Gao, H., Huang, Y., Nix, W. D., and Hutchinson, J. W., 1999, "Mechanism-Based Strain Gradient Plasticity—I. Theory," J. Mech. Phys. Solids, **47**, pp. 1239–1263.
[10] Hutchinson, J. W., 2000, "Plasticity at the Micron Scale," Int. J. Solids Struct., **37**, pp. 225–238.
[11] Ashby, M. F., 1970, "The Deformation of Plastically Non-Homogeneous Alloys," Philos. Mag., **21**, pp. 399–424.
[12] Poole, W. J., Ashby, M. F., and Fleck, N. A., 1996, "Micro-Hardness Tests on Annealed and Work-Hardened Copper Polycrystals," Scr. Metall., **34**(4), pp. 559–564.
[13] Wahl, K., and Asif, S. A., 2000, Naval Research Laboratories, personal communication.
[14] Johnson, K. L., Kendall, K., and Roberts, A. D., 1971, "Surface Energy and the Contact of Elastic Solids," Proc. R. Soc. London, Ser. A, **A321**, pp. 301–313.
[15] Derjaguin, B. V., Muller, V. M., and Toporov, Yu. P., 1975, "Effect of Contact Deformations on the Adhesion of Particles," J. Colloid Interface Sci., **53**, pp. 314–326.
[16] Maugis, D., 1999, "Contact, Adhesion and Rupture of Elastic Solids," *Series in Solid State Sciences*, Springer, New York, pp. 62–66, 283–295.
[17] Tymiak, N. I., Kramer, D. E., Bahr, D. F., and Gerberich, W. W., 2001, "Plastic Strain and Strain Gradients at Very Small Penetration Depths," Acta Mater., **49**, pp. 1021–1034.
[18] Baskes, M., and Horstemeyer, M., 1999, Sandia National Labs, private communication.
[19] Horstemeyer, M. F., and Baskes, M. I., 1999, "Atomistic Finite Deformation Simulations: A Discussion on Length Scale Effects in Relation to Mechanical Stresses," ASME J. Eng. Mater. Technol., **121**, pp. 114–119.
[20] Gane, M., and Cox, J. M., 1970, "The Micro-Hardness of Metals at Very Low Loads," Philos. Mag., **22**(179), pp. 881–891.
[21] Oliver, W. C., and Pharr, G. M., 1992, "An Improved Technique for Determining Hardness and Elastic Modulus Using Load and Displacement Sensing Experiments," J. Mater. Res., **7**(6), pp. 1564–1583.
[22] Stelmashenko, N. A., Walls, M. G., Brown, L. M., and Milman, Yu. V., 1993, "Microindentations on W and Mo Oriented Single Crystals: An STM Study," Acta Metall. Mater., **41**(1), pp. 2855–2865.
[23] Bahr, D. F., Kramer, D. E., and Gerberich, W. W., 1998, "Non-Linear Deformation Mechanisms During Nanoindentation," Acta Mater., **46**(10), pp. 3605–3617.
[24] Gerberich, W. W., Kramer, D. E., Tymiak, N. I., Volinsky, A. A., Bahr, D. F., and Kriese, M. D., 1999, "Nanoindentation-Induced Defect-Interface Interactions: Phenomena, Methods and Limitations," Acta Mater., **47**(15), pp. 4115–4123.
[25] Bobji, M. S., Biswas, S. K., and Pethica, J. B., 1997, "Effect of Roughness on the Measurement of Nanohardness—A Computer Simulation Study," Appl. Phys. Lett., **71**(8), pp. 1059–1061.
[26] Gerberich, W. W., Yu, W., Kramer, D., Strojny, A., Bahr, D., Lilleodden, E., and Nelson, J., 1998, "Elastic Loading and Elastoplastic Unloading from Nanometer Level Indentations for Modulus Determinations," J. Mater. Res., **13**, pp. 421–439.
[27] Begley, M. R., and Hutchinson, J. W., 1998, "The Mechanics of Size-Dependent Indentation," J. Mech. Phys. Solids, **46**, pp. 2049–2068.
[28] Belak, J., and Stowers, I. F., 1992, "The Indentation and Scraping of a Metal Surface: A Molecular Dynamics Study," *Fundamentals of Friction*, I. L. Singer and H. M. Pollock, eds., Kluwer Academic, Dordrecht, pp. 511–520.
[29] Johnson, K. L., 1985, *Contact Mechanics*, Cambridge Univ., Cambridge, UK, Press, pp. 153–184.
[30] Kramer, D., Huang, H., Kriese, M., Robach, J., Nelson, J., Wright, A., Bahr, D., and Gerberich, W. W., 1999, "Yield Strength Predictions from the Plastic Zone Around Nanocontacts," Acta Mater., **47**(1), pp. 333–343.
[31] Binnig, G., Quate, C. F., and Gerber, Ch., 1987, "Atomic Force Microscope," Phys. Rev. Lett., **56**, pp. 930–933.
[32] Kheshgi, H. S., and Scriven, L. E., 1991, "Dewetting, Nucleation and Growth of Dry Regions," Chem. Eng. Sci., **46**, pp. 519–526.
[33] Josell, D., and Spaepen, F., 1993, "Determination of the Interfacial Tension by Zero Creep Experiments on Multilayers," Acta Metall., **41**, pp. 3015–3027.
[34] Vermaak, J. S., and Kuhlman-Wilsdorf, D., 1968, "Measurement of the Average Surface Stress of Gold as a Function of Temperature in the Temperature Range 50–985°," J. Phys. Chem., **72**, pp. 4150–4154.
[35] Mays, C. W., Vermaak, J. S., and Kuhlman-Wilsdorf, D., 1968, "Surface Stress and Surface Tension. II. Determination of the Surface Stress of Gold," Surf. Sci., **12**, pp. 134–140.
[36] Wasserman, H. J., and Vermaak, J. S., 1970, "Determination of a Lattice Contraction in Very Small Silver Particles," Surf. Sci., **22**, pp. 164–172.
[37] Friesen, C., Dimitrov, N., Cammarata, R. C., and Sieradzki, K., 2000, "Surface Stress and the Electrocapilarity of Solid Electrodes," Surf. Sci., submitted for publication.
[38] Gerberich, W. W., Venkataraman, S. K., Huang, H., Harvey, S. E., and Kohlstedt, D. L., 1995, "The Injection of Plasticity by Millinewton Contacts," Acta Metall. Mater., **43**(4), pp. 1569–1576.
[39] Michalske, T. A., and Houston, J. E., 1998, "Dislocation Nucleation at Nano-Scale Mechanical Contacts," Acta Mater., **46**(2), pp. 391–396.
[40] Gerberich, W. W., Nelson, J. C., Lilleodden, E. T., Anderson, P., and Wyrobek, J. T., 1996, "Indentation Induced Dislocation Nucleation: The Initial Yield Point," Acta Mater., **44**(9), pp. 3585–3598.
[41] Fleck, N. A., Muller, G. M., Ashby, M. F., and Hutchinson, J. W., 1994, Acta Metall. Mater., **42**(2), pp. 475–487.
[42] Gouldstone, A., Koh, H.-J., Zeng, K.-Y., Giannakopolous, A. E., and Suresh, S., 2000, "Discrete and Continuous Deformation During Nanoindentation of Thin Films," Acta Mater., **48**, pp. 2277–2295.

[43] Yasuda, K., Shinohara, K., Kinoshita, C. and Arai, M., 1994, ''An Interpretation of the Indentation Size/Load Effect on Diamond Pyramid Hardness,'' *Strength of Materials*, Oikawa et al., eds., The Japan Institute of Metal, pp. 865–868.
[44] Corcoran, S. G., Colton, R. J., Lilleodden, E. T., and Gerberich, W. W., 1997, ''Anomalous Plastic Deformation of Surfaces: Nanoindentation of Gold Single Crystals,'' Phys. Rev. B, **55**(24), pp. 16057–16060.
[45] Cheng, L., 1996, ''Numerical Modeling of Indentation and Scratch Problems,'' Ph.D. Thesis, University of Minnesota.
[46] Couchman, P. R., Jesser, W. A., Kuhlmann-Wilsdorf, D., and Hirth, J. P., 1972, Surf. Sci., **33**, pp. 429–436.
[47] Kramer, D. E., Yoder, K. B., and Gerberich, W. W., 2001, ''Surface Constrained Plasticity: Oxide Rupture and the Yield Point Process,'' Philos. Mag. A, **81**(8), pp. 2033–2058.
[48] Cheng, Y.-T., and Cheng, C.-M., 1998, ''Relationships Between Hardness, Elastic Modulus, and the Work of Indentation,'' Appl. Phys. Lett., **73**(5), pp. 614–616.
[49] Hirth, J., and Loethe, J., 1982, *Theory of Dislocations*, 2nd Ed., John Wiley and Sons, pp. 837–839.